PAPER

Curvature and anisotropy estimation through the CRS approximation

IOP Publishing Journal of Geophysics and Engineering
J. Geophys. Eng. **12** (2015) 934–945 doi:10.1088/1742-2132/12/6/934

Curvature and anisotropy estimation through the CRS approximation

Shibo Xu and Alexey Stovas

Department of Petroleum Engineering and Applied Geophysics, Norwegian University of Science and Technology, S.P. Andersens veg 15a, NO-7491 Trondheim, Norway

E-mail: shibo.xu@ntnu.no and alexey.stovas@ntnu.no

Received 17 March 2015, revised 7 August 2015
Accepted for publication 12 August 2015
Published 26 October 2015

Abstract

Multiparameter stacking is a crucial tool to get a high-quality time image of the subsurface, which can provide a basis for many important applications. We analyse the CRS approximation for a circular reflector embedded into effective anisotropic media. In this case, the CRS attributes depend on both reflector curvature and anisotropy parameters. We consider the effective anisotropic model from two anisotropic cases—elliptical isotropic and transversely isotropic with vertical symmetry axis—and one vertically heterogeneous isotropic case, i.e. two-layer model. By performing a sensitivity analysis, we show how the estimates depend on anisotropy parameters. We convert the CRS attributes into parameters for the isotropic model and analyse these estimates' behaviour along the seismic line. From this behaviour, we estimate both structure and anisotropy parameters.

Keywords: CRS approximation, anisotropy estimation, seismic inversion

(Some figures may appear in colour only in the online journal)

1. Introduction

Stacking plays an important role in seismic data processing, which is treated as one of the fundamental operations in seismic data analysis (Yilmaz 2000). The signal-to-noise ratio can be improved considerably by adopting a multiparameter stacking operator as the information of the same subsurface region is carried from the neighbouring CMP gathers. A number of multiparameter stacking operators have been proposed in recent years. The common-reflection-surface (CRS) method is developed (Jäger *et al* 2001) as an extension of the classical stacking operation, stacking data from multiple CMP locations. The traveltime surface of the CRS method can be described by a hyperbolic approximation from a Taylor series expansion of the squared traveltime around a reference ray. By introducing the concepts of the normal (N) and normal-incident-point (NIP) waves set out by Hubral (1983), the series coefficients can be formulated in terms of three kinematic attributes (Jäger *et al* 2001, Tygel and Santos 2007); these attributes have a clear physical interpretation that can be used for structural interpretation, velocity model estimation for depth migration (Duveneck 2004) and prestack seismic data interpolation (Baykulov and Gajewski 2009). The implicit expression for the reflection traveltime on a spherical reflector derived by Taylor expansion with a fourth-order expansion is presented in Höcht *et al* (1999). The multifocusing (MF) approach, originally developed by Gelchinsky *et al* (1999a, 1999b), is a double square root-based approximation parametrized with the same attributes as the CRS operator in addition to the conventional stacking velocity. The extended approach is modified by Landa *et al* (2010) to provide an analytical solution to the spherical reflector problem and take heterogeneity into consideration. A non-hyperbolic CRS (NCRS) approximation has been proposed to improve the accuracy at the offset and midpoint coordinates with the same set of parameters (Fomel and Kazinnik 2013). A new implicit CRS approach (i-CRS) combining the high sensitivity to the curvature of the MF with the robustness of CRS with respect to inhomogeneity on the circular interface was introduced by Schwarz *et al* (2014). An extended work for i-CRS taking weak-anisotropy into account was done by Vanelle *et al* (2012).

In this paper, we start with the isotropic CRS approximation, then we take anisotropy into consideration, and finally we evaluate the structural and anisotropic parameters. We propose a new approach to investigate the effects of anisotropy and vertical heterogeneity on the P-wave CRS attributes and

their inversion into the model parameters. In order to distinguish between the reflector curvature, anisotropy and heterogeneity, we consider simple circular anisotropic and layered isotropic background models. To describe all these models in the same framework of an effective anisotropic medium, we use the generalized moveout approximation (GMA) proposed by Fomel and Stovas (2010) to define the group velocity as a function of group angle. In order to simplify our method, we assume that the difference between the incidence and reflection phase and the group angles is negligibly small.

A comparison of CRS attributes and inverted model parameters exhibits different behaviour depending on the background model. Considering the estimated model parameters $\hat{R}$ and $\hat{z}_0$ from different midpoint positions, we estimate the effective anisotropy parameters. The CRS attributes being inverted into the model parameters under the isotropic model assumption show a dependence on the position of the midpoint. From these dependences, we can evaluate the parameters of the reflector and anisotropy parameters.

2. CRS approximation for a circular reflector

In order to introduce the effect of reflector curvature, we start with the simplest (circular) reflector embedded in a homogeneous isotropic medium with velocity V. In this case, the traveltime surface can be described by the parametric relations (Höcht *et al* 1999). The model is shown in figure 1 (left). The reflector is given by a circle with a radius R and the centre located at $(0, z_0)$. For the isotropic model, the model parameters are R, V and z_0. The source and receiver lateral coordinates are x_s and x_r, respectively. For a given x_s and x_r, the reflection point is specified by the dip angle α and reflection angle θ (figure 1, left). The coordinates x_s and x_r are given by the geometrical relations as

$$\begin{aligned} x_s &= R\sin\alpha + (z_0 - R\cos\alpha)\tan(\alpha-\theta),\\ x_r &= R\sin\alpha + (z_0 - R\cos\alpha)\tan(\alpha+\theta). \end{aligned} \tag{1}$$

The midpoint, half-offset and the reflection traveltime function can be expressed as

$$\begin{aligned} m &= \frac{x_r + x_s}{2} = R\sin\alpha + (z_0 - R\cos\alpha)\frac{\sin\alpha\cos\alpha}{\cos^2\alpha - \sin^2\theta},\\ h &= \frac{x_r - x_s}{2} = (z_0 - R\cos\alpha)\frac{\sin\theta\cos\theta}{\cos^2\alpha - \sin^2\theta}, \end{aligned} \tag{2}$$

$$\begin{aligned} T &= \frac{(z_0 - R\cos\alpha)}{V\cos(\alpha-\theta)} + \frac{(z_0 - R\cos\alpha)}{V\cos(\alpha+\theta)}\\ &= 2\frac{(z_0 - R\cos\alpha)}{V}\frac{\cos\alpha\cos\theta}{\cos^2\alpha - \sin^2\theta}. \end{aligned} \tag{3}$$

The parametric equations (2) and (3) define the reflection traveltime surface $T(m,h)$. We select a certain midpoint position m_0 and expand the traveltime squared in series for $\Delta m = m - m_0$ and half offset h (figure 2). By expanding the traveltime squared in the Taylor series for Δm and h, we obtain the second order CRS approximation in a form (Jäger *et al* 2001),

$$T^2_{\mathrm{CRS}}(\Delta m, h) = A_0 + A_1\Delta m + A_2\Delta m^2 + B_2 h^2. \tag{4}$$

The series coefficients A_0, A_1, A_2 and B_2 are computed for a given m_0 and depend on the model parameters R, V and z_0.

3. Inversion of the CRS attributes and estimated model parameters

The CRS operator in the simulated zero-offset (ZO) section can be represented in terms of three kinematic wavefield attributes. The parameters R_{NIP} and R_{N} are the radius of the normal incidence and normal waves (Jäger *et al* 2001), and the emergence angle is denoted by β. The meaning of the attributes is illustrated in figure 1 (right). According to the concept of R_{NIP}, R_{N} and β, the series coefficients in equation (4) can be expressed through these CRS attributes.

$$\begin{aligned} A_0 &= \frac{4R^2_{\mathrm{NIP}}}{V_0^2}, A_1 = \frac{8R_{\mathrm{NIP}}\sin\beta}{V_0^2},\\ A_2 &= \frac{4(R_{\mathrm{NIP}}\cos^2\beta + R_{\mathrm{N}}\sin^2\beta)}{V_0^2 R_{\mathrm{N}}}, B_2 = \frac{4\cos^2\beta}{{V_0}^2}. \end{aligned} \tag{5}$$

The CRS attributes can be represented in terms of the model parameters for the isotropic model.

$$R_{\mathrm{NIP}} = z_0\sec\alpha_0 - R, R_{\mathrm{N}} = z_0\sec\alpha_0, \beta = \alpha_0, \tag{6}$$

where α_0 is the incidence angle for a given m_0.

The CRS attributes can be, consequently, given in terms of A_0, A_1, A_2 and B_2.

$$\begin{aligned} \hat{R}_{\mathrm{NIP}} &= \frac{2A_0}{\sqrt{4A_0B_2 + A_1^2}}, \hat{R}_{\mathrm{N}} = \frac{8A_0^2B_2}{(4A_0A_2 - A_1^2)\sqrt{4A_0B_2 + A_1^2}},\\ \sin\hat{\beta} &= \frac{A_1}{\sqrt{4A_0B_2 + A_1^2}}, \end{aligned} \tag{7}$$

and the isotropic model parameters can be defined as

$$\begin{aligned} \hat{R} &= \frac{2A_0(A_1^2 + 4A_0B_2 - 4A_0A_2)}{(4A_0A_2 - A_1^2)\sqrt{4A_0B_2 + A_1^2}}, \hat{V} = \sqrt{\frac{16A_0}{A_1^2 + 4A_0B_2}},\\ \hat{z}_0 &= \frac{16A_0^2B_2\sqrt{A_0B_2}}{(4A_0A_2 - A_1^2)(A_1^2 + 4A_0B_2)}. \end{aligned} \tag{8}$$

All the expressions above are derived for the isotropic case. Therefore, in case of the isotropic model, equation (8) results in exact values for the R, V and z_0.

4. Application of the CRS method for effective anisotropic models

In order to compute the CRS attributes for a circular reflector embedded into an effective anisotropic medium, we use the GMA approximation (Fomel and Stovas 2010) to define the group velocity as a function of group angle. This velocity can later be used in equation (3), replacing the constant velocity V.

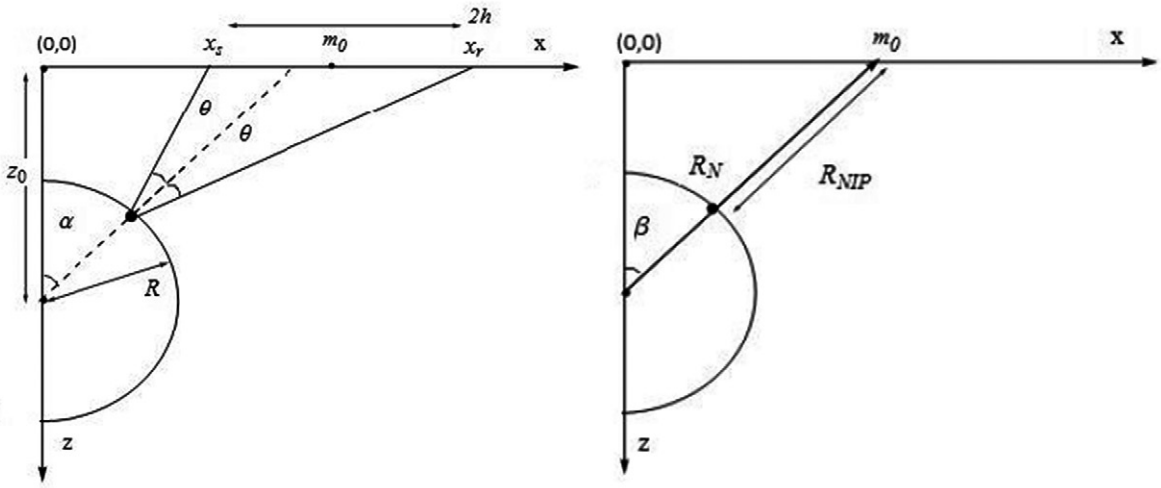

Figure 1. (Left) is the reflection from a circular reflector in a homogeneous medium, (right) is the illustration of the three CRS attributes β, $R_{\rm NIP}$ and $R_{\rm N}$, where β is the emergence angle of the reflector, $R_{\rm NIP}$ is the distance from the reflection point to the surface and $R_{\rm N}$ is the distance from the centre of the reflector to the surface.

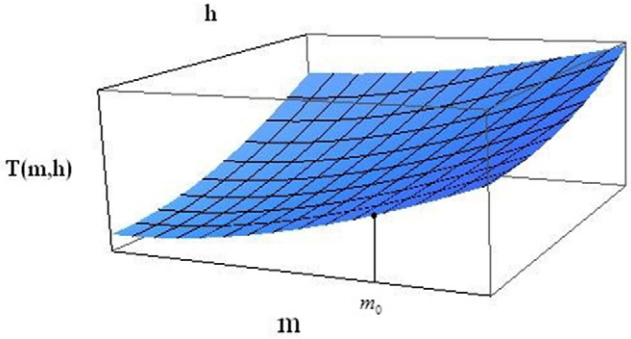

Figure 2. Traveltime surface $T(m,h)$ from a circular reflector and the reference point ($m = m_0$) for the Taylor series expansion (equation (4)).

$$\frac{1}{V(\phi)^2} = \frac{\cos^2\phi}{V_0^2} + \frac{\sin^2\phi}{V_{\rm N}^2} + \frac{A\sin^2\phi\tan^2\phi}{V_{\rm N}^4\left(\frac{1}{V_0^2} + \frac{B\tan^2\phi}{V_{\rm N}^2} + \sqrt{\frac{1}{V_0^4} + \frac{2B\tan^2\phi}{V_0^2V_{\rm N}^2} + \frac{C\tan^4\phi}{V_{\rm N}^4}}\right)}, \tag{9}$$

where V_0 is the vertical velocity, $V_{\rm N}$ is the NMO velocity, the parameters A, B and C are model dependent, and ϕ is the ray propagation angle. The CRS operators related to anisotropy can be obtained by adopting the GMA velocity in anisotropic media.

If the model above the reflector shown in figure 1 (left) is anisotropic, the group velocities for the incoming and outgoing rays are different, and the incidence and reflection phase (or group) angles are also different due to Snell's law. We show that the difference between the incidence and reflection group angles is negligibly small, see appendix A, and the geometrical equations (1) and (2) are still valid for further computation.

Therefore, by adopting the group velocity equation from equation (9), the traveltime equation (3) takes the form

$$T = \frac{(z_0 - R\cos\alpha)}{\cos(\alpha-\theta)}\frac{1}{V(\alpha-\theta)} + \frac{(z_0 - R\cos\alpha)}{\cos(\alpha+\theta)}\frac{1}{V(\alpha+\theta)}. \tag{10}$$

Equation (10) with the velocity defined in equation (9) is more complicated compared with equation (3) defined for the isotropic model. When using equation (9), we have additional parameters ($V_{\rm N}, A, B, C$) that affect the solution. In order to compute the CRS series coefficients A_0, A_1, A_2 and B_2 for the effective anisotropic case in equation (4), we use equations (9) and (10). We adopt a new traveltime equation (10) using the anisotropic group velocity defined by GMA in equation (9) with the same geometry form given in equation (2). The new CRS attributes are obtained by equating the coefficients with equation (4).

We introduce three velocity models: the elliptical isotropic (EI) case with Thomsen parameters $\delta = \varepsilon$ (Thomsen 1986), the transversely isotropic case with a vertical symmetry axis (VTI) and the two-layer isotropic model (2LI).

For the EI case, by setting $A = 0$, the group velocity in equation (9) takes the form

$$\frac{1}{V^2(\phi)} = \frac{\cos(\phi)^2}{V_0^2} + \frac{\sin(\phi)^2}{V_{\rm N}^2}. \tag{11}$$

For the VTI case, the parameters A, B and C in equation (9) given in terms of anelliptic parameter $\eta = (\varepsilon - \delta)/(1 + 2\delta)$ (Alkhalifah 1998) take the form (Fomel and Stovas 2010)

$$A = -4\eta, B = \frac{1 + 8\eta + 8\eta^2}{1 + 2\eta}, C = \frac{1}{(1 + 2\eta)^2}. \tag{12}$$

For the 2LI case, we introduce two layers with velocities V_1 and V_2. The first layer is specified from the surface to the top of the circular reflector. The second layer is beneath the first one (figure 3, top). The kinematical properties of this model depend on the depth for the reflection point. Therefore, for

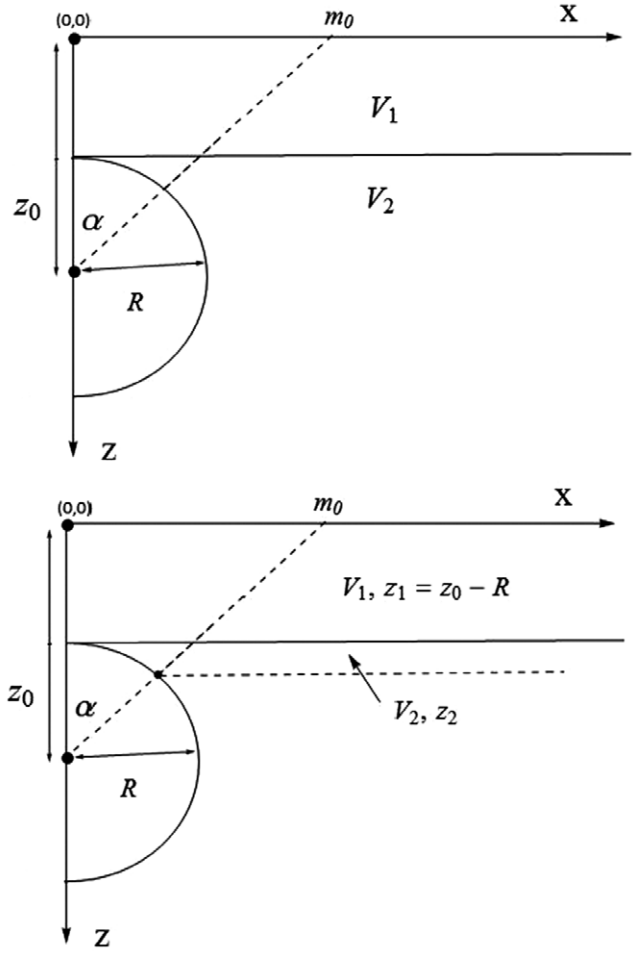

Figure 3. Reflector in the layered isotropic medium (top) and two effective layers (bottom).

each reflection point, we define the parameters V_0, V_N, A, B and C. This means that the velocity model given in equation (9) will be different for different reflection points (figure 3, bottom).

For the 2LI model, the GMA parameters take the form (see appendix B for details):

$$\begin{aligned} V_0 &= V_1 \frac{1+\lambda}{1+\frac{\lambda}{\gamma}}, \\ V_N &= V_1 \sqrt{\frac{1+\lambda\gamma}{1+\frac{\lambda}{\gamma}}}, \\ A &= -\frac{\lambda(\gamma^2-1)^2}{2\gamma(1+\lambda\gamma)^2}, \\ B &= \frac{(\gamma^2-1)\left(1+\frac{\lambda}{\gamma}\right)}{2(1+\lambda\gamma)^2}, \\ C &= 0. \end{aligned} \tag{13}$$

The parameters λ and γ are defined by the ratios, $\lambda = \frac{z_2}{z_1}$, $\gamma = \frac{V_2}{V_1}$, and the parameter λ is related to the model parameters as

$$\lambda = \frac{R(1-\cos\alpha)}{z_0 - R}, \tag{14}$$

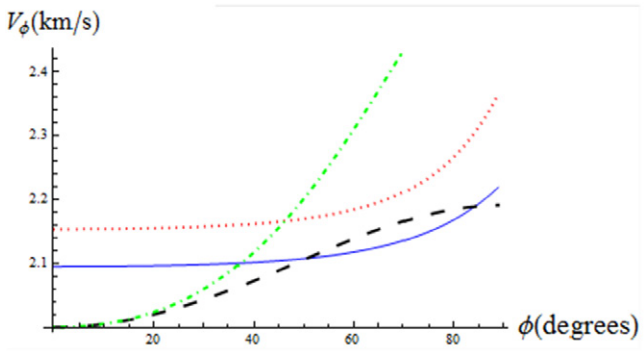

Figure 4. Plot of the GMA group velocity of different models versus group angle ϕ. The 2LI ($m_0 = 2$), 2LI ($m_0 = 4$), EI and VTI cases are shown by solid, dotted, dashed and dot-dashed lines, respectively.

which is controlled by the midpoint position m_0. If the medium is not a homogeneous isotropic one, equations (7) and (8) result in estimates represented by hats that are dependent on the position m_0, where the series coefficients A_0, A_1, A_2 and B_2 are computed.

To illustrate the different velocity models introduced above, we show the group velocity from EI, VTI and two 2LI models. In figure 4, the group velocities are shown as the function of group angle. The velocity model parameters are $R = 1$km, $z_0 = 2$km, $V_0 = 2\text{km s}^{-1}$, $V_N = V_0\sqrt{1+2\delta}$, $\delta = 0.1$, $\eta = 0.2$. For the 2LI model, we select $V_1 = 2\text{km s}^{-1}$, $V_2 = 2.5\text{km s}^{-1}$ and two m_0 positions: $m_0 = 2$km and $m_0 = 4$km, which give $\lambda_1 \approx 0.29$, $\lambda_2 \approx 0.55$ and $\gamma = 1.25$. One can see that the 2LI models result in significantly different behaviour of the group velocity.

5. Influence of effective anisotropy

In order to test our approach and investigate the effect of the anisotropy and inhomogeneity on the CRS attributes and estimated model parameters, we select the circular reflector with parameters $R = 1$ km, $z_0 = 2$ km and four velocity models. The first velocity model is isotropic (ISO) with velocity $V_0 = 2\text{km s}^{-1}$. The EI model has two parameters $V_0 = 2\text{km s}^{-1}$ and $\delta = 0.1$, the VTI model has the same parameters as the EI model plus the anisotropy parameter $\eta = 0.2$ and the parameters for the 2LI model are $V_1 = 2\text{km s}^{-1}$ and $V_2 = 2.5\text{km s}^{-1}$.

First, we compute the coefficients A_0, A_1, A_2 and B_2 for all the models mentioned above. Then, we compute the CRS attributes (equation (7)) and the 'isotropic' model parameters (equation (8)). As stacking is not considered in this paper, the analytical expressions of CRS coefficients A_0, A_1, A_2 and B_2 in effective anisotropic media are not computed here.

In figure 5, we show the series coefficients A_0, A_1, A_2 and B_2 from equation (5) plotted versus m_0 for all the models mentioned above (note that $m_0 = 0$ is the circle centre position). The tendencies of coefficients A_0 and A_1 are similar for all the models, but the behaviour of coefficients A_2 and B_2 for the VTI model is quite different. For all m_0, the largest and the smallest values for series coefficients are obtained from the ISO and VTI models, respectively.

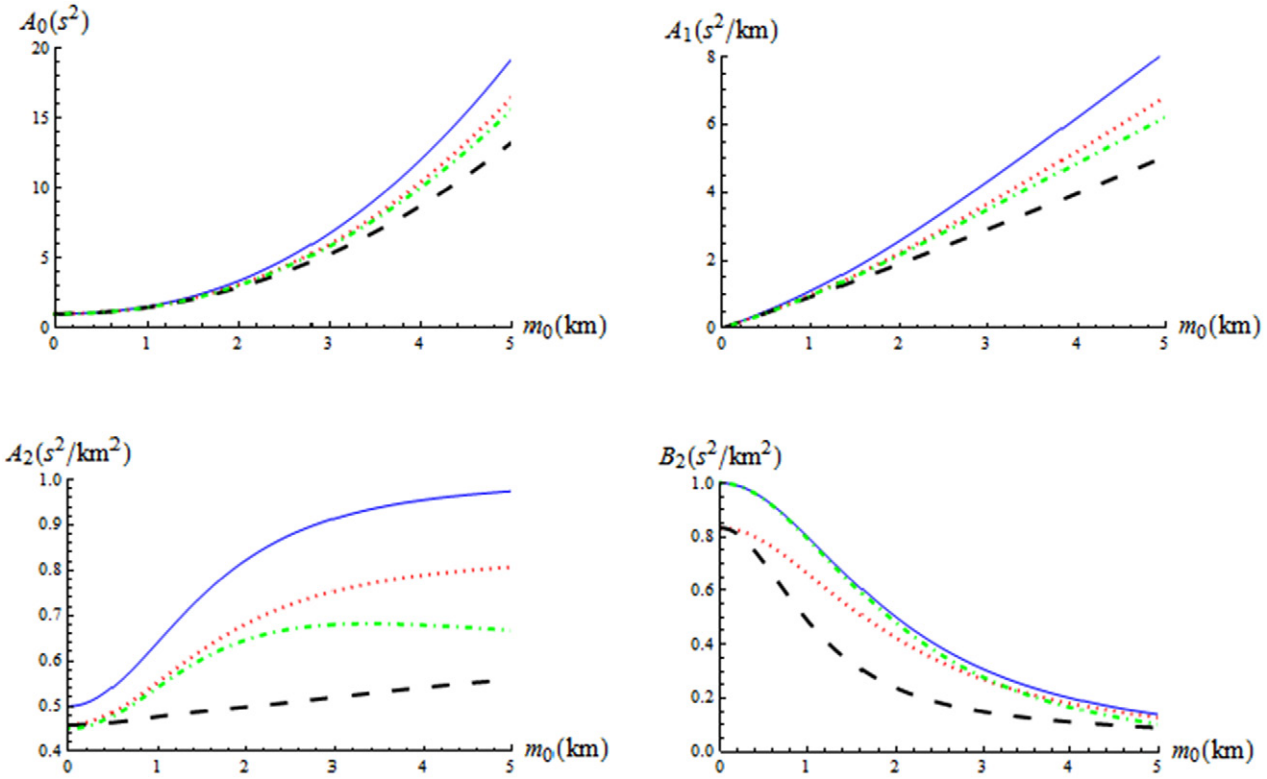

Figure 5. The series coefficients in equation (4) plotted versus m_0. The ISO, EI, VTI and 2LI cases are shown by solid, dotted, dashed and dot-dashed lines, respectively.

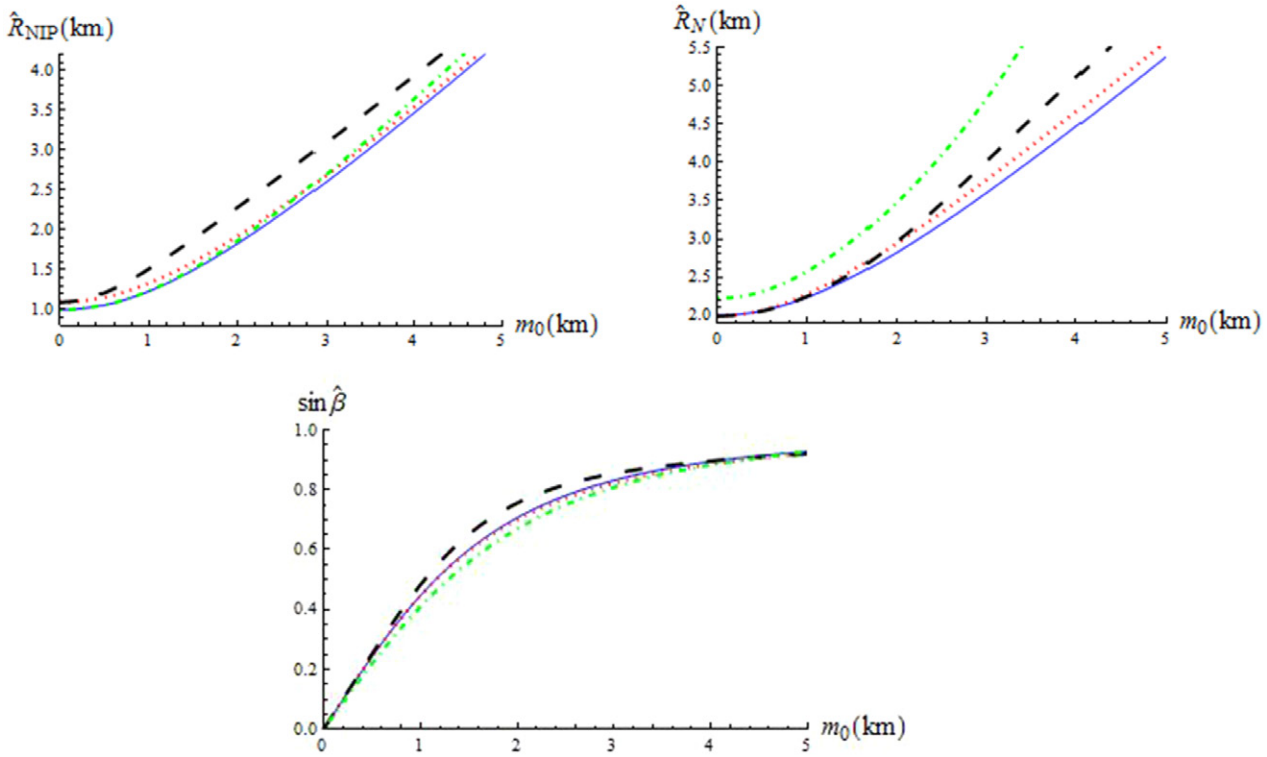

Figure 6. The CRS attributes given in equation (7) and plotted versus m_0. The ISO, EI, VTI and 2LI cases are shown by solid, dotted, dashed and dot-dashed lines, respectively.

The corresponding CRS attributes computed from equation (7) are plotted versus m_0 in figure 6. The tendency for the ISO and EI case is very similar for all attributes, while the VTI and 2LI models result in different attribute behaviour.

The CRS attributes obtained from all the models are converted into the isotropic model parameters by using equation (8). The results are shown in figure 7. One can see that the inversion from isotropic models produces the

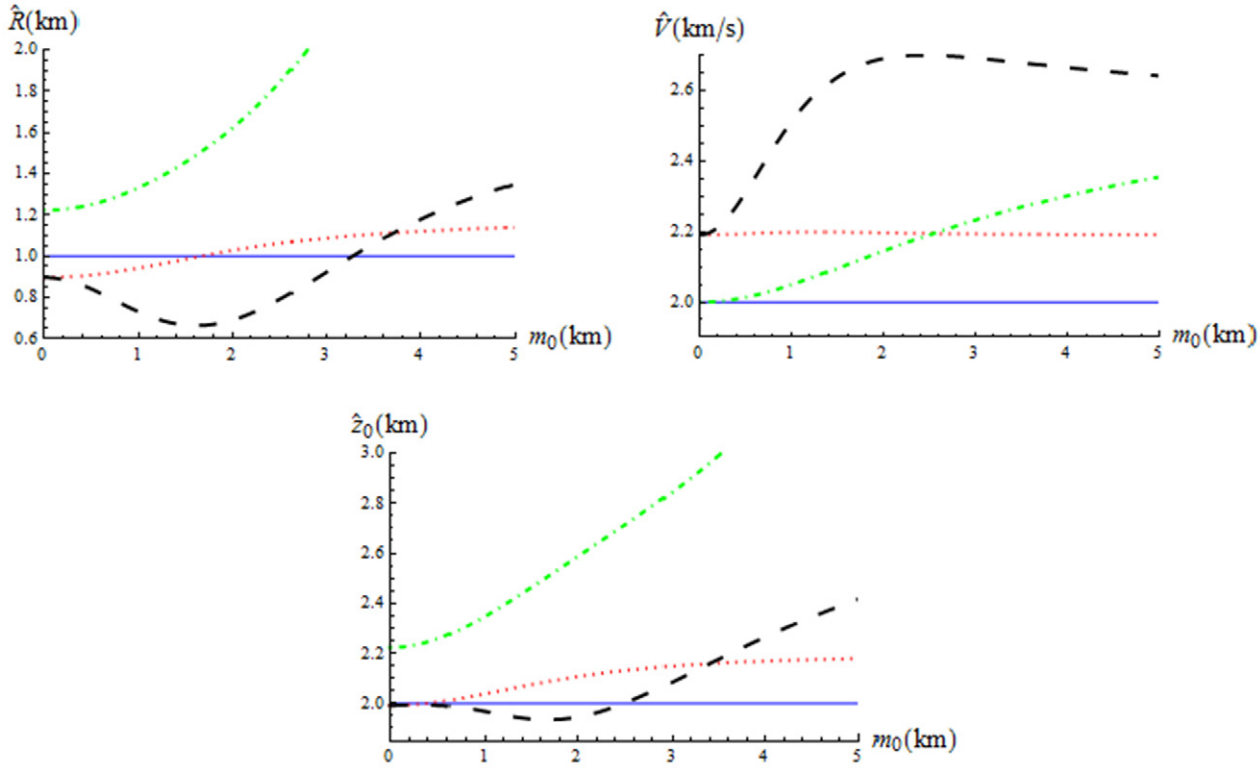

Figure 7. The estimates in the isotropic model parameters in equation (8) plotted versus m_0. The ISO, EI, VTI and 2LI cases are shown by solid, dotted, dashed and dot-dashed lines, respectively.

estimates that are equal to model parameters and do not depend on m_0. All the other models result in estimates that depend on m_0. From the plots in figure 7, we can see the estimated reflector radius, in the presence of anisotropy, is underestimated above the circle and overestimated when the midpoint is far away from lateral position of the circle's centre. In our computation, we use the limit $m_0 \to \infty$. However, in practice, one can use the value when the estimate exhibits asymptotic behaviour. $\hat{z}_0$ is slightly underestimated for a small midpoint and overestimated for a large m_0. For the 2LI model, $\hat{R}$ and $\hat{z}_0$ are overestimated for all m_0. The estimated velocity is larger than the model velocity for all the models.

We also reconstruct the reflection surface by computing the position for each reflection point, $\hat{x} = m_0 - \hat{R}_{\mathrm{NIP}} \sin\hat{\beta}$ and $\hat{z} = \hat{R}_{\mathrm{NIP}} \cos\hat{\beta}$. The shape of the surface obtained from the estimates computed from the different models is shown in figure 8. To reconstruct all these surfaces, we use the range of $m_0 \in (0, 5\ \mathrm{km})$. The most dramatic difference in the shape of the reflector compared with the circle is obtained for the VTI case. The EI model results in a shape that is very similar to a circle with a different radius. The 2LI model gives a shape which is very similar to the circle, but which deviates slightly for larger emergence angles.

Diffraction plays an important role in seismic processing and interpretation. In order to investigate the effects of diffraction in our approach, we set $R = 0$ (point diffractor) and perform a similar analysis to the one above (see appendix C).

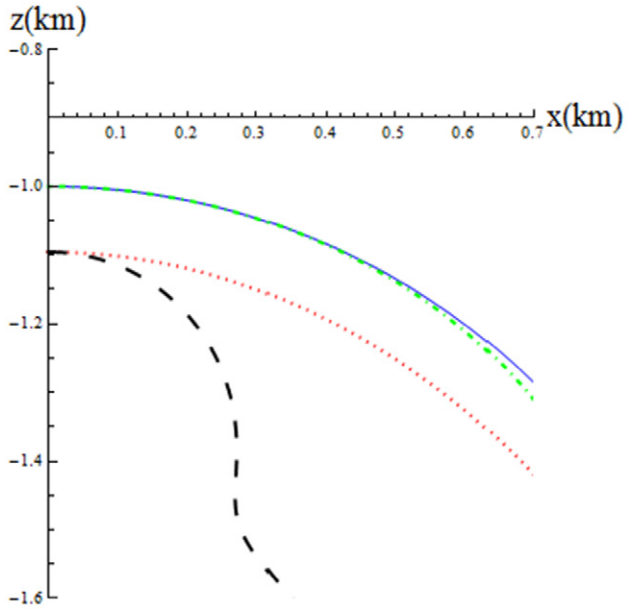

Figure 8. The reconstructed shape of the reflector based on the estimations of $\hat{R}_{\mathrm{NIP}}(m_0)$ and $\sin\hat{\beta}(m_0)$ for different models. The ISO, EI, VTI and 2LI cases are shown by solid, dotted, dashed and dot-dashed lines, respectively.

6. Curvature and anisotropy estimation

For a VTI model, we can linearize the CRS attributes and estimated model parameters in terms of anisotropy parameters δ and η. These results are shown in appendix D.

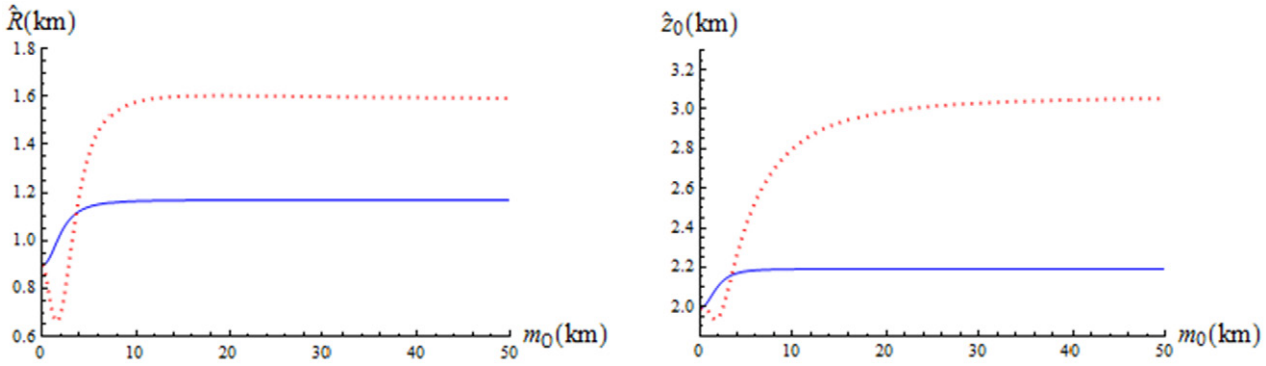

Figure 9. Plot of the estimated radius (left) and depth for the centre of a circular reflector (right) plotted versus m_0. The EI and VTI cases are shown by solid and dotted lines, respectively.

The behaviour of estimated parameters $\hat{R}$, $\hat{V}$ and $\hat{z}_0$ is controlled by anisotropy parameters δ and η. As shown in figure 9, the estimated radius and depth for the EI and VTI models approach an asymptotic value when m_0 goes to infinity. When m_0 equals zero, these values are the same since the anelliptic parameter η does not affect the vertical wave propagation. This allows us to estimate $\hat{R}$ and $\hat{z}_0$ along with the anisotropy parameters.

The results of $\hat{R}$ and $\hat{z}_0$ in zero and infinite limit are specified by $\hat{R}^{(0)} = \hat{R}(m_0 = 0)$, $\hat{R}^{(\infty)} = \hat{R}(m_0 \to \infty)$, $\hat{z}_0^{(0)} = \hat{z}_0(m_0 = 0)$ and $\hat{z}_0^{(\infty)} = \hat{z}_0(m_0 \to \infty)$.

For the EI model, in the weak-anisotropy approximation (small δ), the estimated $\hat{R}$ varies from $R(1-\delta)$ at $m_0 = 0$ to $R(1+2\delta)$ at $m_0 \to \infty$. Therefore, the anisotropy parameter δ and radius R can be evaluated from the variation of $\hat{R}$ with m_0. The expressions of $\hat{R}^{(0)}$ and $\hat{R}^{(\infty)}$ are given by

$$\hat{R}^{(0)} = \lim_{m_0 \to 0} \hat{R} = R\left(\frac{z_0 + 2R\delta - 2z_0\delta}{z_0 + 2R\delta}\right)\sqrt{1+2\delta} \approx R(1-\delta), \tag{15}$$

$$\hat{R}^{(\infty)} = \lim_{m_0 \to \infty} \hat{R} = R\frac{1+4\delta}{1+2\delta} \approx R(1+2\delta). \tag{16}$$

The estimation for the curvature and anisotropy parameter can be obtained from the inversion of equations (15) and (16).

$$\widetilde{R} = \frac{2\hat{R}^{(0)} + \hat{R}^{(\infty)}}{3}, \widetilde{\delta} = \frac{\hat{R}^{(\infty)} - \hat{R}^{(0)}}{2\hat{R}^{(0)} + \hat{R}^{(\infty)}}. \tag{17}$$

For the VTI case, the results of $\hat{R}$ and $\hat{z}_0$ in zero and infinite limit are given as follows

$$\hat{R}^{(0)} = \lim_{m_0 \to 0} \hat{R} = R\left(\frac{z_0 + 2R\delta - 2z_0\delta}{z_0 + 2R\delta}\right)\sqrt{1+2\delta} \approx R(1-\delta), \tag{18}$$

$$\hat{R}^{(\infty)} = \lim_{m_0 \to \infty} \hat{R} = R\left(2 - \frac{1}{(1+2\delta)(1+2\eta)^2}\right) \approx R(1+2\delta+4\eta), \tag{19}$$

$$\hat{z}_0^{(0)} = \lim_{m_0 \to 0} \hat{z}_0 = \frac{z_0^2\sqrt{1+2\delta}}{z_0 + 2R\delta} \approx z_0(1+\delta) - 2R\delta, \tag{20}$$

Table 1. Comparison of the structural and anisotropy parameters made between the VTI model parameters and the estimates.

	R(km)	z_0 (km)	δ	η
VTI model parameters	1.0	2.0	0.1	0.2
Estimates	0.941	1.987	0.048	0.084

$$\hat{z}_0^{(\infty)} = \lim_{m_0 \to \infty} \hat{z}_0 = z_0\sqrt{1+2\delta}(1+2\eta) \approx z_0(1+\delta+2\eta). \tag{21}$$

The anisotropy parameters δ, η, radius and depth can be inversed from equations (18)–(21).

For the real data, we do not have measurements taken at the infinite midpoint position. Instead, we are going to use the data from $m_0 = 5$ km. From the estimates we obtained from a VTI model, $\hat{R}^{(0)} = 0.896$ km, $\hat{R}^{(\infty)} = 1.348$ km, $\hat{z}_0^{(0)} = 1.992$ km and $\hat{z}_0^{(\infty)} = 2.417$ km. Using these estimates in equations (18)–(21) results in $R = 0.941$ km, $z_0 = 1.987$ km, $\delta = 0.048$ and $\eta = 0.084$ (see the comparison in table 1). The circular reflector parameters are estimated very well, but the anisotropy parameters are underestimated. The reason for this is the original anisotropy parameters are very large for using weak-anisotropy approximation equations (18)–(21). For real data, one can use the optimization searching for the CRS attributes by fitting the operators, then using this inversion method to estimate the geophysical information (curvature, depth and anisotropy parameters).

7. Conclusions

Based on the CRS approximation, we propose a new method to evaluate the anisotropy parameters and the circular reflector parameters from the behaviour of estimates with the midpoint position m_0 for a circular reflector. We consider two anisotropic models and a two-layer isotropic model, which we treat in the same framework of effective anisotropic media by using the GMA for group velocity.

In the presence of anisotropy, the estimated reflector curvature is overestimated from the midpoints just above the circle and underestimated when the midpoints are far away from the circle. The estimated depth for the centre of the circular reflector is underestimated above the reflector and

overestimated for far away midpoints. Both the estimated depth and radius are overestimated for the 2LI model. By analysing the variations in the estimated model parameters computed for anisotropic media versus the midpoint position, we can evaluate both the structural and anisotropic parameters. Despite not knowing the lateral position of the circular object, we can estimate and plot the estimated attributes (computed in the vicinity of each m_0) as a function of m_0. From these functions, the lateral position of the object can be clearly seen.

Acknowledgments

We would like to acknowledge the ROSE project and the China Scholarship Council (CSC) for financial support.

Appendix A. Incidence and reflection group angle

In the case of a circular reflector in a homogeneous anisotropic velocity model (figure A1), the velocity varies with the wave propagation direction. For the EI case ($\delta = \varepsilon$), the phase velocity for the P-wave is given by (Alkhalifah and Tsvankin 1995)

$$V_P(\theta) = V_{P0}\sqrt{1 + 2\delta \sin^2\theta}, \tag{A.1}$$

where V_{P0} is the vertical velocity, θ is the phase angle and δ is the Thomsen (1986) anisotropy parameter. The expression for group velocity is

$$\frac{1}{V_P^2(\phi)} = \frac{\cos^2\phi}{V_{P0}^2} + \frac{\sin^2\phi}{V_N^2}, \tag{A.2}$$

ϕ is the ray/group angle, V_N is the NMO velocity being $V_N = V_{P0}\sqrt{1+2\delta}$.

Snell's law is derived from the plane wave propagation and is valid in the phase domain. The form for Snell's law is the following,

$$\frac{\sin\theta_1}{\sin\theta_2} = \frac{V_P(\theta_1)}{V_P(\theta_2)}, \tag{A.3}$$

with θ_1 and θ_2 being the incidence and reflection phase angle.

The relation for the incidence and reflection group angles in the EI model can be obtained after a tedious computation from equations (A.1)–(A.3) and takes the form

$$\tan\phi_2 = \frac{\tan\phi_1(1+2\delta)(\delta\cos 2\alpha - \delta - 1)}{2\delta^2\cos 2\alpha + 2\tan\phi_1\delta\sin 2\alpha + \delta\cos 2\alpha - 2\delta^2 - 3\delta - 1}, \tag{A.4}$$

where ϕ_1 is the incidence group angle, ϕ_2 is the reflection group angle and α is the dip angle.

From equation (A.4), one can see that the behaviour of the difference group angle $\Delta\phi$ is controlled by ϕ_1, α and δ.

The difference between the reflection and incidence group angles $\Delta\phi = \phi_2 - \phi_1$ is shown versus the incidence group angle ϕ_1 and the reflector dip angle α in figure A2 for $\delta = 0.1$ (top) and $\delta = 0.2$ (bottom). One can see that for moderate incidence angles, the difference is small, and we neglect this in our derivations.

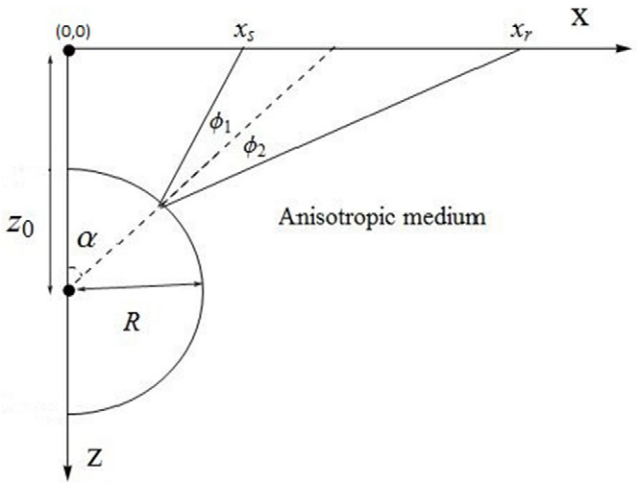

Figure A1. The reflection from a circular reflector in a homogeneous anisotropic medium.

Appendix B. CRS approximation in the 2LI model

In order to analyse the effects of heterogeneity, we introduce a two-layer model, with the first layer being adjusted to the top of circular reflector (figure 3, top). We introduce an effective artificial layer with the thickness from the reflection point to the top of the circular reflector. The offset and moveout of the 2LI model can be represented in terms of horizontal slowness,

$$x(p) = \frac{2z_1pV_1}{\sqrt{1-p^2V_1^2}} + \frac{2z_2pV_2}{\sqrt{1-p^2V_2^2}}, \tag{B.1}$$

$$t(p) = \frac{2z_1}{V_1\sqrt{1-p^2V_1^2}} + \frac{2z_2}{V_2\sqrt{1-p^2V_2^2}}. \tag{B.2}$$

From equations (B.1) and (B.2), we can compute all the parameters of the GMA approximation in equation (9).

It is convenient to express the GMA parameters in terms of the thickness and velocity ratios for $\lambda = \frac{z_2}{z_1}$ and $\gamma = \frac{V_2}{V_1}$ as follows

$$V_0 = V_1\frac{1+\lambda}{1+\frac{\lambda}{\gamma}}, V_N = V_1\sqrt{\frac{1+\lambda\gamma}{1+\frac{\lambda}{\gamma}}}, A = -\frac{\lambda(\gamma^2-1)^2}{2\gamma(1+\lambda\gamma)^2}. \tag{B.3}$$

The other parameters are defined from a horizontal ray in layer one. It gives

$$B = \frac{t_0^2(1-V_N^2p_\infty^2)}{t_0^2 - T_\infty^2} - \frac{A}{1-V_N^2p_\infty^2} = \frac{(\gamma^2-1)\left(1+\frac{\lambda}{\gamma}\right)}{2(1+\lambda\gamma)^2},$$
$$C = \left(\frac{t_0^2(1-V_N^2p_\infty^2)}{t_0^2 - T_\infty^2}\right)^2 = 0. \tag{B.4}$$

Appendix C. Diffraction case

The diffraction case can be considered as a special case of the circular reflector by setting $R = 0$ (figure C1). In terms of CRS attributes, it gives $R_N = R_{NIP}$.

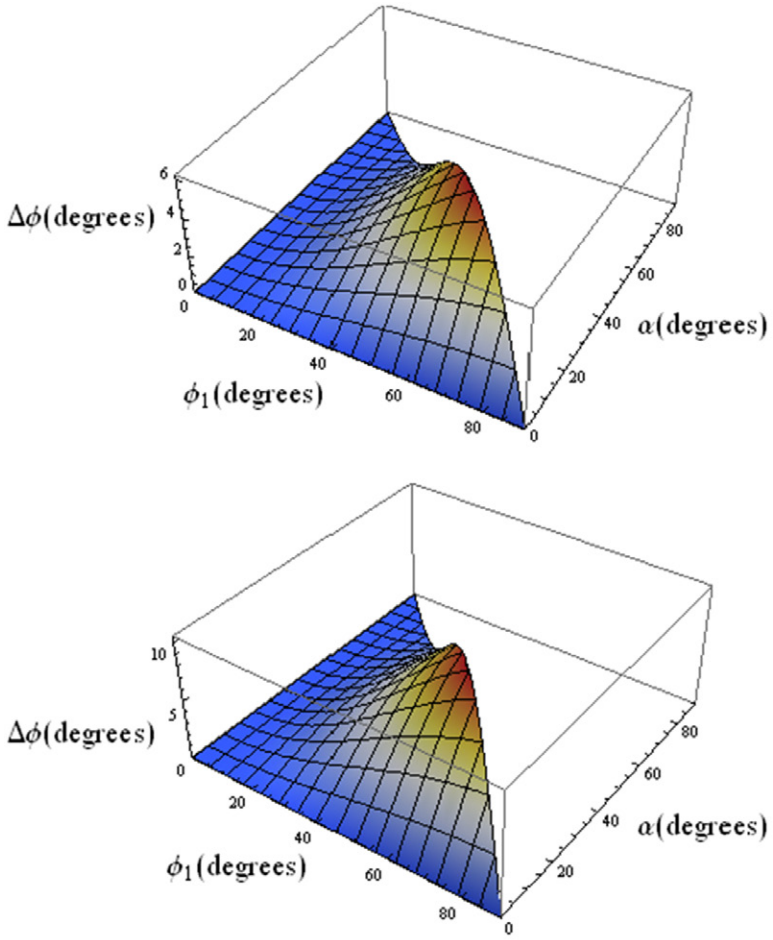

Figure A2. The difference between the reflection and incidence group angles in the EI model plotted versus ϕ_1 and α ($\delta = 0.1$ top, $\delta = 0.2$ bottom), $\phi_1 + \alpha \leqslant \frac{\pi}{2}$.

By setting $R = 0$ in equations (2) and (3), we obtain the double square root (DSR) equation,

$$T = \frac{1}{V}\sqrt{z_0^2 + (m+h)^2} + \sqrt{z_0^2 + (m-h)^2}. \qquad \text{(C.1)}$$

If the point diffractor is embedded into the anisotropic model, equation (C.1) becomes

$$T = \frac{\sqrt{z_0^2 + (m-h)^2}}{V_1} + \frac{\sqrt{z_0^2 + (m+h)^2}}{V_2}, \qquad \text{(C.2)}$$

$V_1 = V\left(\phi = \tan^{-1}\left(\frac{m_0 - h}{z_0}\right)\right)$ and $V_2 = V\left(\phi = \tan^{-1}\left(\frac{m_0 + h}{z_0}\right)\right)$, where $V(\phi)$ is defined in equation (9).

When applying the inversion equation (8) for the anisotropic velocity models, we observe that $\hat{R} = 0$ regardless of the anisotropic parameters. This means that the presence of anisotropy does not result in smearing of the point diffractor.

The CRS attributes computed from equation (C.2) are shown in figure C2. The plot for $\sin\hat{\beta}$ is very similar for all three cases. The estimated $\hat{R}_{\rm N}(\hat{R}_{\rm NIP})$ in the VTI case is larger than the one estimated from the other cases.

In figure C3, we show the estimated model parameters $\hat{V}$ and $\hat{z}_0$ for the point diffractor plotted versus m_0. The value

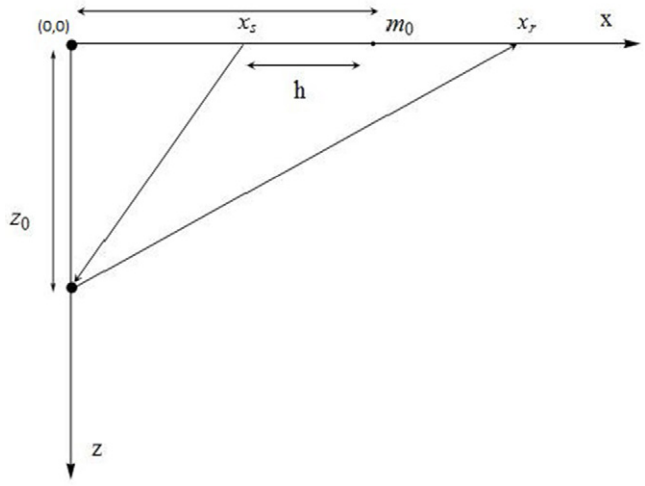

Figure C1. The point diffractor in a homogeneous medium.

for the estimated velocity and depth in the EI case does not depend on m_0. For the VTI case, the estimated velocity and depth exhibit a strong variation with m_0.

The estimated $\hat{z}_0$ for the point diffractor in the VTI model varies from $z_0\sqrt{1+2\delta}$ at $m_0 = 0$ to $z_0\sqrt{1+2\delta}(1+2\eta)$ at

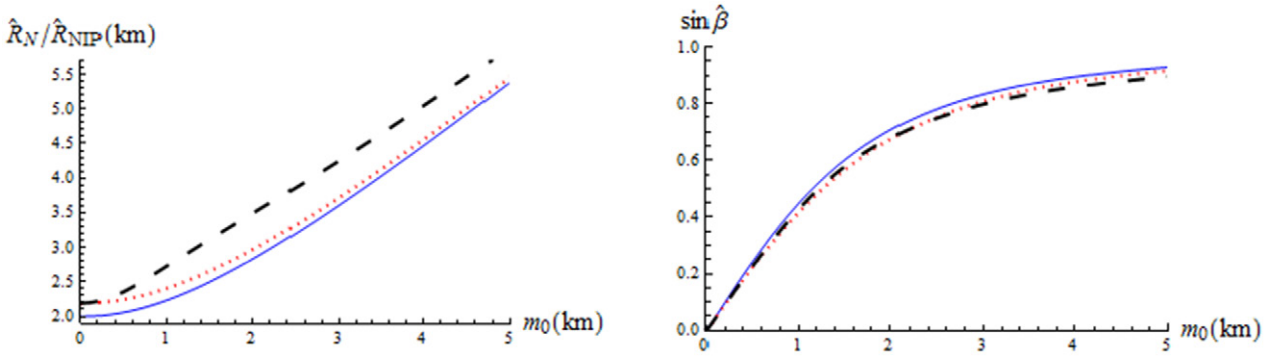

Figure C2. The CRS attributes for a point diffractor plotted versus m_0. The ISO, EI and VTI cases are shown by solid, dotted and dashed lines, respectively.

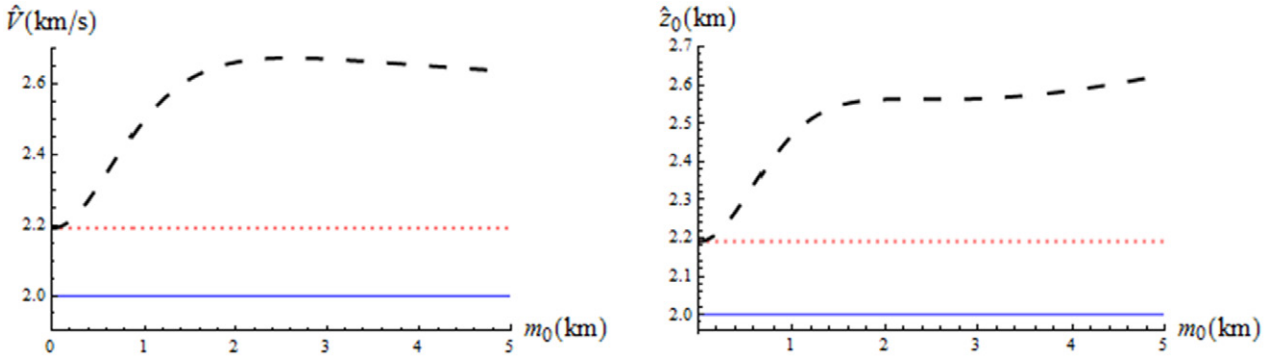

Figure C3. The estimated model parameters for a point diffractor plotted versus m_0. The ISO, EI and VTI cases are shown by solid, dotted and dashed lines, respectively.

$m_0 \to \infty$. This variation can be used as an indicator for anelliptic parameter η.

Appendix D. Sensitivity analysis

In the case of a circular reflector embedded into the anisotropic velocity model, the CRS attributes and estimated model parameters depend on the anisotropy parameters.

In order to perform the sensitivity analysis, we linearize $\hat{R}_{NIP}$, $\hat{R}_N$, $\sin\hat{\beta}$ and $\hat{R}$, $\hat{V}$, $\hat{z}_0$ in terms of anisotropy parameters δ and η.

The expressions for the CRS attributes take the form,

$$\hat{R}_{NIP} = \left(\sqrt{m_0^2+z_0^2} - R\right)\left(1 + \frac{z_0^2}{m_0^2+z_0^2}\delta + \frac{2m_0^2z_0^2(m_0^2+3z_0^2)}{(m_0^2+z_0^2)^3}\eta\right), \tag{D.1}$$

$$\hat{R}_N = \sqrt{m_0^2+z_0^2}\left(1 + \frac{z_0^2\left(\sqrt{m_0^2+z_0^2}-2R\right)+2m_0^2R}{(m_0^2+z_0^2)^{3/2}}\delta + \frac{6m_0^2z_0^2\left(z_0^2-2R\sqrt{m_0^2+z_0^2}\right)+2m_0^4\left(z_0^2+2R\sqrt{m_0^2+z_0^2}\right)}{(m_0^2+z_0^2)^3}\eta\right), \tag{D.2}$$

$$\sin\hat{\beta} = \frac{m_0}{\sqrt{m_0^2+z_0^2}}\left(1 - \frac{z_0^2\left(\sqrt{m_0^2+z_0^2}-2R\right)}{(m_0^2+z_0^2)^{3/2}}\delta + \frac{2m_0^2z_0^2\left(z_0^2-m_0^2+2R\sqrt{m_0^2+z_0^2}\right)}{(m_0^2+z_0^2)^3}\eta\right). \tag{D.3}$$

For the estimated model parameters, the analytical expressions are given in the form

$$\hat{R} = R\left(1 + \frac{2m_0^2-z_0^2}{m_0^2+z_0^2}\delta + \frac{2m_0^2(2m_0^4-3m_0^2z_0^2-3z_0^4)}{(m_0^2+z_0^2)^3}\eta\right), \tag{D.4}$$

$$\hat{V} = V_0\left(1+\delta + \frac{m_0^2(m_0^4+3m_0^2z_0^2+6z_0^4)}{(m_0^2+z_0^2)^3}\eta\right), \tag{D.5}$$

$$\hat{z}_0 = z_0\left(1 + \frac{(m_0^2+z_0^2)^2 - 2z_0^2R\sqrt{m_0^2+z_0^2}}{(m_0^2+z_0^2)^2}\delta + \frac{2m_0^2\left(m_0^4+3z_0^4-6Rz_0^2\sqrt{m_0^2+z_0^2}\right)}{(m_0^2+z_0^2)^3}\eta\right). \tag{D.6}$$

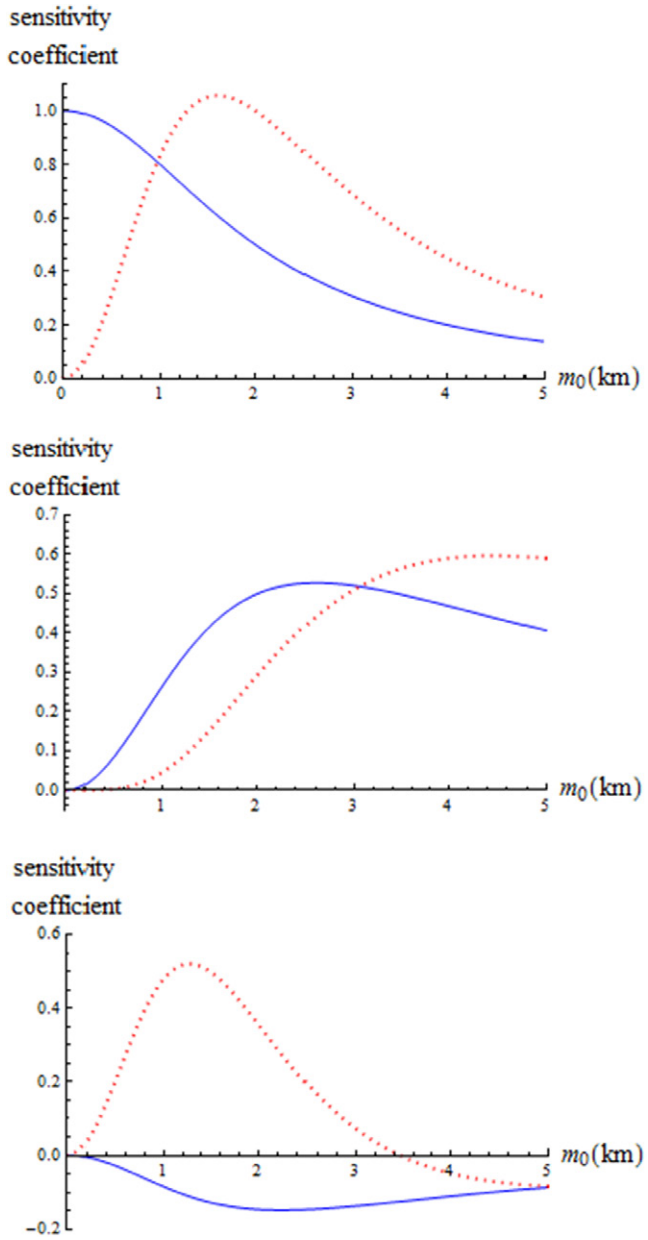

Figure D1. The sensitivity coefficients for anisotropy parameters δ and η, shown by solid and dotted lines, respectively, and plotted versus m_0. The corresponding CRS attributes are $\hat{R}_{\mathrm{NIP}}$ (top), $\hat{R}_{\mathrm{N}}$ (middle) and $\sin\hat{\beta}$ (bottom).

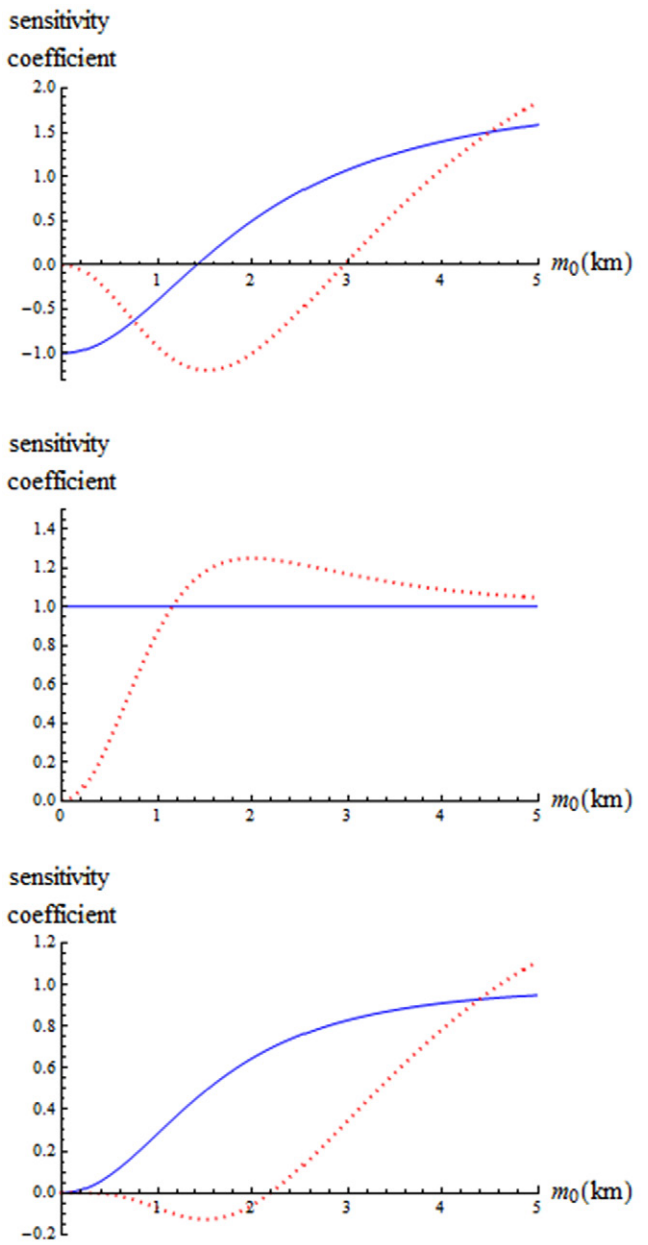

Figure D2. The sensitivity coefficients for anisotropy parameters δ and η, shown by solid and dotted lines, respectively, and plotted versus m_0. The corresponding estimates for isotropic model parameters are $\hat{R}$ (top), $\hat{V}$ (middle) and $\hat{z}_0$ (bottom).

The sensitivity coefficients for anisotropy parameters δ and η computed for the CRS attributes and estimated model parameters are plotted versus m_0 in figures D1 and D2, respectively.

From figure D1, we can see that the effect of parameter δ is predominant over the effect of parameter η for $\hat{R}_{\mathrm{NIP}}$ and $\hat{R}_{\mathrm{N}}$ when m_0 is small (the lateral CMP position is close to the position of the centre of a circular reflector). The presence of anisotropy results in overestimating the CRS parameters $\hat{R}_{\mathrm{NIP}}$ and $\hat{R}_{\mathrm{N}}$. The parameter δ results in the underestimation of $\sin\hat{\beta}$ for moderate values of m_0.

From figure D2, we can see that for small m_0, $\hat{R}$ is underestimated due to the presence of anisotropy, while $\hat{V}$ is overestimated. The contribution of parameter δ into $\hat{V}$ does not depend on m_0, see equation (D.5). For large m_0, the presence of anisotropy results in the overestimation of $\hat{z}_0$. For all estimations, the effect of anellipticity parameter η is very small for a small value of m_0.

References

Alkhalifah T 1998 Acoustic approximations for processing in transversely isotropic media *Geophysics* **63** 623–31

Alkhalifah T and Tsvankin I 1995 Velocity analysis for transversely isotropic media *Geophysics* **60** 1550–66

Baykulov M and Gajewski D 2009 Prestack seismic data enhancement with partial common-reflection-surface (CRS) stack *Geophysics* **74** V49–58

Duveneck E 2004 Velocity model estimation with data-derived wavefront attributes *Geophysics* **69** 265–74
Fomel S and Kazinnik R 2013 Non-hyperbolic common reflection surface *Geophys. Prospect.* **61** 21–7
Fomel S and Stovas A 2010 Generalized nonhyperbolic moveout approximation *Geophysics* **75** U9–18
Gelchinsky B, Berkovitch A and Keydar S 1999a Multifocusing homeomorphic imaging—Part 1 Basic concepts and formulae *J. Appl. Geophys.* **42** 229–42
Gelchinsky B, Berkovitch A and Keydar S 1999b Multifocusing homeomorphic imaging: II. Multifold data set and multifocusing *J. Appl. Geophys.* **42** 243–60
Höcht G, de Bazelaire E, Majer P and Hubral P, 1999 Seismics and optics: hyperbolae and curvatures *J. Appl. Geophys.* **42** 261–81
Hubral P 1983 Computing true amplitude reflections in a laterally inhomogeneous earth *Geophysics* **48** 1051–62
Jäger R, Mann J, Höcht G and Hubral P 2001 Common-reflection-surface stack: image and attributes *Geophysics* **66** 97–109
Landa E, Keydar S and Moser T J 2010 Multifocusing revisited: inhomogeneous media and curved interfaces *Geophys. Prospect.* **58** 925–38
Schwarz B, Vanelle C, Gajewski D and Kashtan B 2014 Curvatures and inhomogeneities: an improved common reflection surface approach *Geophysics* **79** S231–40
Thomsen L 1986 Weak elastic anisotropy *Geophysics* **51** 1954–66
Tygel M and Santos L T 2007 Quadratic normal moveouts of symmetric reflections in elastic media: a quick tutorial *Studia Geophys. Geod.* **51** 185–206
Vanelle C, Bobsin M, Schemmert P, Kashtan B and Gajewski D 2012 i-CRS: a new multiparameter stacking operator for an/isotropic media *82nd Annual Int. Meeting SEG Expanded Abstracts*
Yilmaz O 2000 Seismic data analysis society of exploration *Geophysicists*